Received: 18 January 2025 | Revised: 1 July 2025 | Accepted: 2 July 2025

DOI: 10.1002/ppp3.70085

Plants People Planet PPP Open Access

RESEARCH ARTICLE

Quantifying urban tree canopy cooling capacity using Bayesian hierarchical models and satellite imagery

Ángel Ruiz-Valero[1] | Jaime Francisco Pereña-Ortiz[1] | Isidro Martín-Lozano[1] | Álvaro Cortés-Molino[2] | Pablo Cozano-Pérez[1] | Begoña Galindo-Ruiz[1] | Luis Alberto Díaz-Galiano[1] | Ángel Enrique Salvo-Tierra[1]

[1]Department of Botany and Plant Physiology, Faculty of Sciences, Universidad de Málaga, Málaga, Spain

[2]Centre de Ciencia i Tecnologia Forestal de Catalunya (CTFC), Lleida, Spain

Correspondence
Jaime Francisco Pereña-Ortiz, Department of Botany and Plant Physiology, Faculty of Sciences, Universidad de Málaga, 29010 Málaga, Spain.
Email: jperena@uma.es

Funding information
Ministry of Education, Professional Formation and Sport of Spain, Grant/Award Number: FPU22/00067; Technological Corporation of Andalusia, Grant/Award Number: 8.06/5.03.6083; Ministry of Education, Professional Formation and Sport of Spain, in the Program of University Teaching Program (Formacion de Profesorado Universitario, FPU)

Societal Impact Statement

Cities are getting hotter because of climate change and urban development, increasing risks to health and well-being. We analyzed how increasing urban tree canopy cover in city areas of 900 m^2 can reduce land surface temperatures, using detailed aerial-LiDAR and satellite data with Bayesian hierarchical models. It was observed that an increase in tree canopy cover produces a cooling effect irrespective of the conditions of the urbanized environment. The goal is to support policymakers and decision-makers with insights to strategically incorporate urban trees into planning frameworks, fostering sustainable, resilient, and healthy urban environments, and advancing climate change adaptation efforts.

Summary

- The urban heat island phenomenon significantly affects thermal comfort in cities. Urban trees offer ecosystem services that can help cool built-up areas, making cities more livable environments. Regarding the cooling capacity associated with increasing urban trees canopy cover, it is often analyzed at the city level. This study aimed to quantify the local-scale cooling benefits of increasing tree canopy cover to inform urban planning.
- Using Landsat 8 satellite imagery to measure land surface temperature, we applied a Bayesian hierarchical models (BHMs) with Integrated Nested Laplace Approximation (R-INLA) to estimate cooling effects in 900 m^2 urban units, accounting for other factors and spatial autocorrelation through a Gaussian field.
- The model achieved a root mean squared error of 0.989°C ± 0.255°C and 0.833 ± 0.06 of observations were covered by the Highest Posterior Probability Interval of the Posterior Predictive Distribution (p-PPD-HPDI), both metrics calculated in the test sets of 10-folds spatial cross-validation. Considering other factors responsible of land surface temperature distribution and spatial autocorrelation using a Gaussian field, the model shows that increasing canopy cover in an observational

unit by 450 m^2 is associated with a reduction of about 0.268°C ($Quantile_{0.025}$ 0.241, $Quantile_{0.975}$ 0.295), ceteris paribus.

- These findings highlight the significant local cooling potential of urban tree planting at scales relevant to planning decisions. By quantifying these effects, the study underscores the value of integrating tree canopy increase into urban design and policy to enhance comfort, resilience, and overall urban sustainability.

KEYWORDS
Bayesian hierarchical model, ecosystem services, remote sensing, urban forestry, urban greening

1 | INTRODUCTION

Urban extent, that is, land cover dominated by man-made materials and infrastructures, constitutes the main land use on which populations live and develop their activities. Currently, almost 57.7% of the global population resides in urban areas. Global urban growth trends indicate that urban areas will continue to expand in the coming decades, with 67.9% of the world's population projected to live in urban centers by 2050 (UN, 2025). Urban growth transforms land use systems, with significant implications for biodiversity and the environment because of (1) the consumption of vast amounts of raw materials (Huang et al., 2018), (2) fragmentation of ecosystem and substitution of natural and seminatural areas by impervious surfaces (Seto et al., 2012), (3) exacerbation of climate change (Houghton et al., 2012), (4) modification of hydrological cycles and biogeochemical cycles (Flintrop et al., 1996), and (5) modification of surface energy balance which implies the development of urban heat islands (UHIs) (Phelan et al., 2015).

UHIs are defined as an urban climate phenomenon by which urban areas experience higher temperatures than adjacent suburban and rural ones (Oke et al., 2017). In the last decades, thermal remote sensing has been used as a method to measure the land surface temperature (LST) (Imhoff et al., 2010). LST has been shown to be highly correlated with air temperature in scientific literature, constituting a valid variable to study UHIs and their intensities (Kim & Brown, 2021). The UHIs calculated by LST and their intensities are defined, respectively, as surface urban heat island (SUHI) and surface urban heat island intensity (SUHII) (Imhoff et al., 2010). There is an extensive body of literature regarding SUHI detection at global scale, and there exists a consensus that urban growth and land cover are the primary factors modulating the formation of SUHIs, as they lead to heat accumulation and an increase in longwave radiation emitted from the surface (Voogt & Oke, 2003).

Thermal comfort in cities will be reduced because of the rising temperatures associated with climate change (IPCC, 2023) which will exacerbate UHIs. Rosenzweig et al. (2018) projected temperature increases of 1.4–3.1°C for 153 cities worldwide by the 2050s and 1.7–5.0°C by the 2080s. Integrated studies on climate change and urban growth show greater increases in UHI intensity compared to studies that analyze these factors independently (Chapman et al., 2017). Additionally, the intensity of heatwaves will be further exacerbated in urban areas because of their interaction with UHIs (Founda & Santamouris, 2017). This synergy amplifies adverse climatic comfort conditions in cities, leading to higher water and energy consumption, increased carbon dioxide emissions, and worsening air pollution, thereby compromising public health and comfort (Li et al., 2019).

These challenges highlight the urgent need for effective adaptation and mitigation measures to address the environmental issues faced by cities, aligning with Sustainable Development Goal 11, which focuses on making human settlements safe, resilient, and sustainable (UN, 2023). The scientific literature has explored numerous alternatives to make city environments more comfortable (Buyantuyev & Wu, 2010; Yu et al., 2020). Urban green spaces, especially when integrated into the Urban Green Infrastructure Network (UGI), are widely acknowledged as a key strategy for mitigating the negative effects of climate change in urban environments by providing essential ecosystem services (ES) (European Commission, 2020). UGI enhances thermal comfort by offering shade and reducing radiation from surfaces (Picot, 2004). It also increases air humidity and lowers sensible heat through evapotranspiration processes (Oke et al., 2017). Moreover, UGI intercepts and stores rainwater, filters runoff, and extracts soil moisture, thereby boosting storage and infiltration capacity during rainfall events (Stovin et al., 2008). Furthermore, UGI plays a vital role in regulating air quality by absorbing pollutants and increasing the deposition of contaminants and particles (Beckett et al., 1998; Bolund & Hunhammar, 1999).

UGIs consist of various components, with the urban forest, defined as the population of trees in a city, being recognized as a central element. Planting urban trees presents a significant opportunity to mitigate high temperatures, and compared to other strategies, it is relatively simple and cost-effective to implement (Marando et al., 2022). A substantial body of literature highlights temperature reductions at the city scale resulting from tree planting, and many cities have already set targets of achieving 30% tree canopy coverage in the 3–30–300 rule (Nieuwenhuijsen et al., 2022). The estimated temperature reductions associated with increased tree canopy cover vary widely, ranging from negligible effects to nearly a 3°C decrease in air temperature. These variations depend on factors such as the percentage of canopy increase, observational units, estimation models and methods, and local climate conditions (Iungman et al., 2023; Krayenhoff et al., 2021; Marando et al., 2022; Rosenzweig et al., 2009).

Cooling capacity has been extensively studied using regression models (Hou & Estoque, 2020; Iungman et al., 2023; Kong et al., 2014; Marando et al., 2022) and more recently through machine

learning models (ML) (Logan et al., 2020). However, standard regression models do not account for spatial autocorrelation in the response variable, which can lead to overly optimistic confidence intervals for fixed effects (Anderson, 1954; Shaikh et al., 2021). In the case of ML, despite significant advances in interpretable ML, challenges persist when estimating effects and functional relationships, particularly when predictors are correlated and not properly included in the model (Molnar, 2022). Additionally, city-level estimates provide a broad overview of the benefits of increasing tree canopy coverage but fail to deliver localized estimates of the temperature reduction effects. As a result, it is crucial to provide territorial planners with estimates at a local scale, which aligns with the scope of urban interventions and processes. Therefore, this study aims to quantify the cooling capacity of urban tree canopy using remote sensing LST data and uncertainty quantification within a Bayesian framework at an operational scale of 900 m^2. The model allows for assessing how local-scale interventions, such as increasing tree canopy coverage, can reduce LST in urban environments while accounting for uncertainty. Our ultimate goal is to inform policymakers and decision-makers about the benefits of strategically integrating urban trees into urban planning to foster sustainable, resilient, and healthy urban environments, while also contributing to climate change adaptation efforts.

2 | MATERIALS AND METHODS

2.1 | Study area

Malaga has a population of 586,770 inhabitants making it the sixth most populous city in Spain (NIE, 2023). It is a coastal city with warm summers and mild winters, with a mean annual temperature of 19.0°C and a mean annual total precipitation of 494.9 mm (NIE, 2022). Attending to Köppen classification, Malaga has a hot-dry-summer Mediterranean climate (Csa) (Beck et al., 2023). Malaga is divided into 11 municipal districts, of which Bailen–Miraflores (D1), Cruz de Humilladero (D2) and Teatinos Universidad (D3), located in the northwestern part of the city, constitute the study area for the present work (Figure 1). These districts are home to 32.4% of Málaga's population, specifically 61,629 inhabitants in D1 (10.5%), 86,352 inhabitants in D2 (14.7%), and 41,983 inhabitants in D3 (7.2%). Regarding public urban trees, Málaga has a total of 104,690 inventoried trees. D1 has 4051 trees (3.87%), D2 has 14,750 trees (14.08%), and D3 has 13,036 trees (12.45%). This means that 30.4% of Málaga's urban trees are in the study area. Considering the usable urban matrix area per district, that is, the urban matrix area excluding the footprint of buildings and roads, D1, D2 and D3 have 14.4, 18.36, and 25.21 trees/ha, respectively.

2.2 | Method

Figure 2 presents a graphical flowchart illustrating the data sources and methods used to estimate the cooling capacity of urban tree canopy cover.

2.2.1 | Tree canopy cooling capacity estimation

Landsat 8 land surface temperature retrieval

Landsat 8 satellite image was downloaded from Earth-Explorer U.S. Geological Survey (USGS), in a post-heatwave date (19/08/2022).

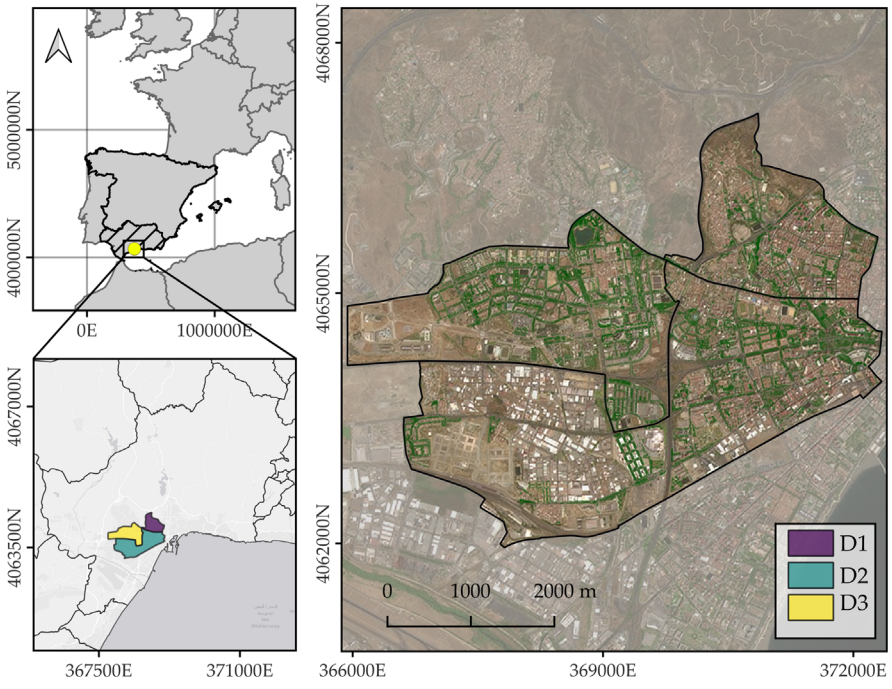

FIGURE 1 Geographic location of the study area. The background information includes data from the Spanish National Geographic Institute for the boundaries of Spain and its municipalities. The orthophotography used is from the 2022 National Plan for Aerial Orthophotography project (NIG, 2022). Green areas indicate the locations of urban tree canopy. Map represented in coordinate reference system: EPSG 25830.

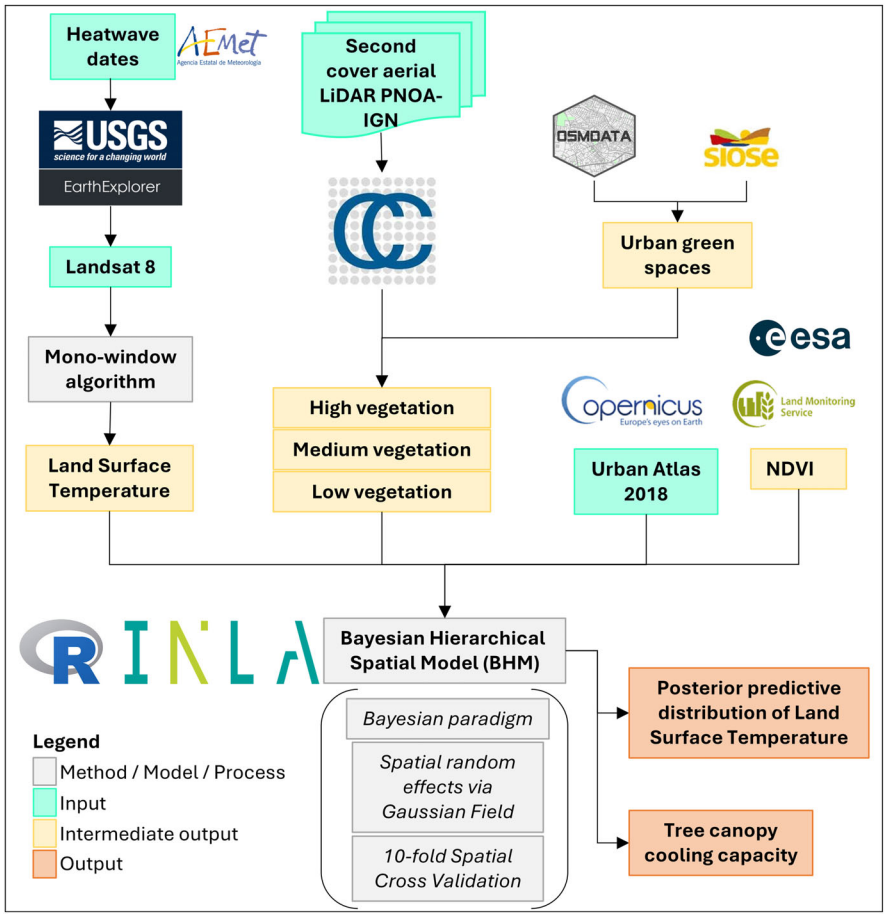

FIGURE 2 Flowchart summary of the developed methodology for estimating tree canopy cooling capacity.

Landsat 8 images have a temporal resolution of 16 days, a spatial resolution of 30 m for the multispectral bands, and a native spatial resolution of 100 m for the thermal bands, which are delivered by USGS at 30-m resolution after cubic convolution resampling (Wulder et al., 2022). The images were sourced from Collection 2 Tier 1, both at Level 1 top-of-atmosphere (TOA) radiance and Level 2 surface reflectance (SR). LST was extracted from Landsat 8 TOA band 10 (10.60–11.19 μm) using the single-channel method described in Jiménez-Muñoz and Sobrino (2003). The method involves the following steps:

1. Convert digital numbers to TOA radiance (Equation 1)

$$L_\lambda = M_L Q_{cal} + A_L \quad (1)$$

where, L_λ is TOA-radiance, M_L represents the band-specific multiplicative rescaling factor from the satellite metadata, Q_{cal} is the band 10 image, and A_L represents the band-specific additive rescaling factor from the satellite metadata.

2. Convert TOA-radiance to brightness temperature using Equation 2

$$BT = \frac{K_2}{\ln\left[\left(\frac{K_1}{L_\lambda}\right)+1\right]} - 273.15 \quad (2)$$

where K_1 and K_2 stand for the band-specific thermal conversion constants from the metadata. For obtaining the results in Celsius, the radiant temperature is revised by adding the absolute zero (approximately − 273.15°C).

3. Correct for land surface emissivity (LSE, ε) via NDVI-based correction. LSE stands for the surface ability that transforms heat energy into radiant energy. According to Sekertekin and Bonafoni (2020), the simplified NDVITHM (THresholds Method) LSE model from Sobrino et al. (2008) provided the best performance to extract LST for all Landsat missions and LST methods. The method involves calculating Normal Difference Vegetation Index (NDVI) and proportion of vegetation (Pv) (Equation 3) for determining ε,

$$P_v = \left(\frac{NDVI - NDVI_s}{NDVI_v - NDVI_s}\right)^2 \quad (3)$$

for application in global conditions, it is suggested using NDVI values for vegetation and soil of $NDVI_v = 0.5$ and $NDVI_s = 0.2$, respectively.

The emissivity (ε) is calculated using Equation (4).

$$\varepsilon_\lambda = \begin{cases} \varepsilon_s\lambda, & NDVI < NDVI_s \\ \varepsilon_s\lambda + (\varepsilon_v\lambda - \varepsilon_s\lambda)P_v, & NDVI_s \le NDVI \le NDVI_v, \\ \varepsilon_v\lambda, & NDVI > NDVI_v \end{cases} \quad (4)$$

where ε_v and ε_s are the vegetation and soil emissivities. When the NDVI is less than 0, it is classified as water, and the emissivity value of 0.991 is assigned. For NDVI values between 0 and 0.2, it is considered that the land is covered with soil, and the emissivity value of 0.996 is assigned. Values between 0.2 and 0.5 are considered mixtures of soil and vegetation. In the final case, when the NDVI value exceeds 0.5, the area is considered to be covered with vegetation, and a value of 0.973 is assigned.

4. Equation (5) is used to calculate LST by emissivity correction on brightness temperature

$$LST = \frac{BT}{1 + \left[\left(\frac{\lambda BT}{\rho}\right) \ln \varepsilon_\lambda\right]} \quad (5)$$

where *LST* is the land surface temperature in Celsius (°C), BT is at-sensor brightness temperature (°C), λ is the wavelength of emitted radiance (for which the peak response and the average of the limiting wavelength [$\lambda = 10.895$] is used), ε_λ is the emissivity calculated in Equation (4), and *p* is calculated by Equation (6)

$$\rho = \frac{hc}{\sigma} = 1.438 \times 10^{-2}\, m\, K, \quad (6)$$

where σ is the Boltzmann constant (1.38×10^{-23} J/K), h is Planck's constant (6.626×10^{-34} J s), and c is the velocity of light (2.998×10^{8} m/s).

Environmental covariables

In the proposed model, LST was considered the response variable. Each observational unit was defined based on Landsat pixels, represented as grid cells with a spatial resolution of 30 × 30 m, equivalent to an area of 900 m^2. Higher-resolution covariates were aggregated to match the spatial scale of these observational units. Eight covariates were initially selected to represent the various factors influencing the distribution of LST.

1. Variables related to urban and vegetation structure were derived from Second Cover aerial LiDAR data from PNOA with a point density of 1.5 points/m^2 (NIG, 2022). For each observational unit, mean building height, total building area, mean tree height, and tree canopy cover were calculated and used as inputs for the model. The cloud points were processed in CloudCompare v.2.12.4 software, and raster height information for low vegetation, medium vegetation, high vegetation, and artificial surfaces was exported as independent files. Urban tree canopies were considered as high vegetation with a minimum of 5 m. Medium and low vegetation were aggregated into a single class because of high noise levels for these land cover types in the cloud points. Building and high vegetation footprints were extracted using height data derived from LiDAR processing and cadastral information for the buildings (SEC, 2025).
2. NDVI, derived from the same satellite image as the LST in its SR version, was included as a covariate to account for the photosynthetic condition of the vegetation.
3. Urban Atlas 2018 was used as the land use land cover (LULC) database for the study area after previous reclassification on the following categories: *continuous urban fabric S.L. > 80%*, *continuous urban fabric S.L. 50–80%*, *continuous urban fabric S.L. 30–50%*, *continuous urban fabric S.L. 10–30%*, *roads*, *water surfaces*, *vacant land*, *industrial surfaces*, *and green spaces*. LULC variable was one-hot encoded. Green spaces were selected as the baseline category.
4. Grass and vacant land area were calculated via the integration of multiple databases, being medium and low vegetation derived from aerial LiDAR the basal data. OpeenStreetMap data were retrieved via de osmdata R package (v. 0.1.9) (Padgham et al., 2017). The following key and values were selected from the API: *landuse – allotments*, *farmland*, *farmyard*, *flowerbed*, *forest*, *meadow*, *orchard*, *vineyard*, *cemetery*, *grass*, *greenfield*, *recreation ground*, *and village green*; *natural – fell*, *grassland*, *heath*, *scrub*, *wood*, *and wetland*; *and*, *leisure – garden*, *nature reserve*, *and park*. The generated spatial database was further reclassified in *vacant land with shrubs or grasslands*, *shrubs*, *woodland*, *grass*, *and green spaces*. SIOSE-AR 2017 (NIG, 2017) was used as a local LULC database to complement Open Street Map information. Green spaces of both databases were further included in the already created LULC covariable. Surface of grass land and vacant land for each observational unit was calculated as covariates for the model. The interest of those variables is to account for the possible effect of the substrate on LST spatial distribution and therefore the cooling capacity of the canopy cover. *Other artificial surfaces cover* for each observational unit was not included to avoid collinearity issues because of compositional data type (simplex, i.e. covariables measured as percentages or proportions summing up to 100% or 1).

To avoid correlation and collinearity among explanatory variables, Pearson's correlation coefficient and the variance inflation factor (VIF) were calculated prior to model implementation. Specifically, correlation was assessed using a Pearson's correlation test with the corrplot package in R (v.0.92) (Wei & Simko, 2024). Collinearity was evaluated by computing the generalized variance inflation factors (GVIF), which adjust the VIF values based on the degrees of freedom of each predictor variable. GVIF was determined using the car R package (v. 3.0–12) (Fox & Weisberg, 2019). Pairs of variables with high correlation (Pearson's $r > 0.6$) or high GVIF (GVIF > 5) were identified, and only one variable from each pair was included in the model. None of the covariates had a VIF greater than 5. NDVI was the only variable exhibiting a correlation higher than 0.6, specifically a value of 0.65 with the tree canopy area. For the final model, NDVI was excluded from this pair of variables, as tree canopy area more accurately represents cooling capacity.

Model specification

Bayesian Hierarchical Models (BHMs) are extensively applied in spatial statistics because of their ability to account for spatial autocorrelation, a phenomenon in which observations closer in space tend to be more strongly correlated than those farther apart (Diggle & Ribeiro, 2007). This is achieved by incorporating Gaussian fields (GFs) as random effects within the model structure (Banerjee et al., 2014). Properly accounting for spatial autocorrelation is critical, as ignoring these dependencies can result in overly narrow credibility intervals and biased relative importance of model coefficients (Lennon, 2000). A Latent Gaussian Model (LGM), understood as a type of BHM with additive structure of the linear predictor and observed data modeled through likelihood depending solely on the value of the linear predictor, was implemented via the Integrated Nested Laplace Approximation framework (INLA) with the INLA R package (v.22.12.16) (Rue et al., 2009).

INLA uses the Stochastic Partial Differential Equations (SPDE) approach, as introduced by Lindgren et al. (2011), to model spatial effects efficiently. The SPDE approach provides an approximation of a continuously indexed GF with a Matérn covariance function by representing it as a discrete zero-mean Gaussian Markov Random Field (GMRF). The finite element method (FEM) is used to solve the SPDE in spatial modeling (Lindgren et al., 2011). This method partitions the study area D into a set of non-intersecting triangles using a Delaunay triangulation, resulting in a mesh consisting of N. The mesh serves as the foundation for constructing N piecewise linear basis functions, denoted as $\varphi(s)$ to approximate the solution to the SPDE. The following parameters were used to define the INLA mesh: (1) prior range, set to 1266 m, corresponding to one fifth of the maximum distance between the X–Y coordinate sets. (2) The maximum allowed triangle edge length in the Delaunay triangulation was set to one fifth of the prior range (253.2). (3) The minimum distance between points was defined as one fifth of the largest allowed triangle edge length (50.64).

The model structure can be summarized as shown in Equation (7)

$$
\begin{aligned}
Y(s_i) \mid \eta_i, \phi &\sim \text{Gaussian}\,(\eta_i, \phi) \\
\eta_i &= \alpha + \sum_{k=1}^{K} \beta_k X_{ik} + u_i \\
\mathbf{U}\{u_i\} &\sim \text{GF}(0, \boldsymbol{\Sigma}) \\
\boldsymbol{\Sigma} &= \begin{pmatrix} c_{11} & c_{12} & \dots & c_{1i} \\ c_{21} & c_{22} & \dots & c_{2i} \\ \vdots & \vdots & \ddots & \vdots \\ c_{j1} & c_{j2} & \dots & c_{ij} \end{pmatrix} \\
c(s_i, s_j) &= \sigma^2 \frac{2^{1-\nu}}{\Gamma(\nu)} \left(\frac{\sqrt{8\nu}\,\| s_i - s_j \|}{\rho} \right)^{\nu} \mathrm{K}_{\nu} \left(\frac{\sqrt{8\nu}\,\| s_i - s_j \|}{\rho} \right)
\end{aligned}
\tag{7}
$$

where $Y(s_i)$ represents the value of the response variable at location s_i; ϕ represents the precision of the normal distribution of the data (likelihood); η_i is the value of the linear predictor for observation i, which, in this case, corresponds to the mean of the likelihood because of identity link function usage; α is the intercept of the model; $\boldsymbol{\beta}$ $\{\beta_k\}$ are the fixed linear effects for each of the k predictors in the model. The coefficient β for canopy cover represents the linear cooling effect on LST associated with an increase in tree canopy coverage within an observational unit, that is, if negative, the decrease of LST owing to canopy cover increase; X_{ik} represents the value of predictor k for observation i; U_i is the random effect for observation i, which is modeled from a GF **U**. It has a zero mean and a spatially structured covariance matrix defined by a set of elements C (s_i,s_j), which models the degree of spatial correlation between positions (s_i,s_j). The covariance matrix is defined by the Matérn covariance function, where Γ is the Gamma function; ρ is the range, defined as the distance at which the correlation is approximately 0.13; σ is the marginal standard deviation; v is the smoothing parameter; and K_v is the modified Bessel function of the second kind of order v. The fixed effects follow a normal prior distribution with precision equal to 0,001. The precision of the likelihood follows a Gamma prior distribution. For the range and marginal standard deviation, a joint prior distribution with penalized complexity prior (PC) is specified. The PC prior is weakly informative and penalizes complexity by shrinking the Matérn spatial range parameter toward infinity, and the marginal standard deviation and error precision toward zero (Fuglstad et al., 2019). It is assumed that the range has a 0.5 probability of being less than 1266, and the marginal standard deviation has a 0.5 probability of being greater than 2.

Because of the approximation of GF by a GMRF in INLA-SPDE, it is represented as piecewise linear basis functions expansion (Equation 8),

$$
\begin{aligned}
\mathbf{Y} \mid \boldsymbol{\beta}, \mathbf{u}, \phi &\sim \text{Gaussian}\,(\boldsymbol{\eta}, \phi) \\
\boldsymbol{\eta} &= \boldsymbol{X\beta} + \boldsymbol{Au} \\
\boldsymbol{u} \sim GF(0, \boldsymbol{\Sigma}) &\sim U(s) = \sum_{j=1}^{N} \phi_j(s)\, w_j
\end{aligned}
\tag{8}
$$

where N is the number of vertices of the mesh, ϕ_j denotes the piecewise linear basis function j, and **W** is the weight vector for each observation associated with each basis function. This implementation modifies slightly the structure in Equation (7) because of the incorporation of a projection matrix **A** which enables the transformation of the GMRF U(s) at the nodes of the mesh to the rest of the observational units in the study area.

Model selection and validation

Spatial cross-validation (CV) was applied with a 10-fold partitioning method to assess model prediction performance. Blocking was generated by blockCV package v2.1–4 (Valavi et al., 2019) with 850 m obtained from the range of the exponential semivariogram adjusted on the response variable and the numeric predictors with gstat R package v.2.0–7 (Pebesma, 2004). Model selection was performed to compare models with and without SPDE component, while keeping the same fixed effects, priors, blocking structure, and observation segregation between the training and test sets. This approach enables the assessment of the added value of incorporating spatial structures in explaining the variability of the response variable. Selection was based on the Watanabe Akaike Information Criterion (WAIC) through the spatial CV process. WAIC is a metric for predictive accuracy and

an approximation to the results of leave-one-out CV. It considers goodness-of-fit and a penalty term that is based on the complexity of the model via the estimated effective number of parameters (Watanabe, 2010).

The model was formally evaluated to assess its overall prediction and generalization capability by calculating R^2, root mean squared error (RMSE), and the proportion of observations covered by the highest posterior density interval (HPDI) of the posterior predictive distribution (p-HPDI-PPD) in the test sets of the spatial-CV scheme. Their mean and standard deviation are reported. R^2 measures the degree of variability explained by the model. RMSE is essentially the standard deviation of the model's errors, that is, the difference between the observed value and its prediction, understood as the mean value of the posterior distribution of the linear predictor for each observation. p-HPDI-PPD represents the number of observations in the test sets, relative to the total size of the set, for which HPDI of the PPD includes the observed value. HPDI can be defined as the narrowest credible interval (i.e., based on a probability distribution, it represents the possible range of values for a parameter given a specified probability mass) that contains the specified probability mass, meaning that all points within this interval have a higher probability density than any points outside the interval. In Bayesian framework, inferences about unknown observables (e.g., new observations for the model) are typically referred to as predictive inferences, as the distribution pertains to a quantity that is observable rather than latent. Given an observation y_i, the PPD is the distribution of the values of y_i generated by the model, conditional on the data already observed. The PPD can be understood as an average of the model's conditional predictions for new data, weighted by the posterior distribution of the model parameters, which allows for accounting uncertainty in parameter estimation (Gelman et al., 2013).

3 | RESULTS

3.1 | Model results

The model with the SPDE exhibited a WAIC of 14,168 ± 591 (i.e., mean ± standard deviation calculated for the 10-model adjusted in the 10-fold spatial CV). The model without the SPDE component reported a WAIC of 57,925 ± 846. The addition of the spatial component in the model dramatically improves the predictive performance of the model. Model without SPDE component took 24.63 s to complete the spatial CV framework. Model with SPDE required 58.71 s. It was concluded that computational time was not an issue of concern with this model because of the favorable computational characteristics of INLA-SPDE method.

The final INLA-SPDE model reported an R^2 of 0.637 ± 0.185 attending to the test sets of the spatial CV scheme. RMSE reported a value of 0.989°C ± 0.255°C, which accounts that in average the predictions almost deviate 1°C from the observed LST. The p-PPD-HPDI shows a value of 0.833 ± 0.06. It indicates that 83% of the observations in every test set ($n = 3808$) are correctly predicted by the model and its uncertainty is contained in its respective PPD. Metrics reflect the ability of the model to correctly predict LST values in the presence of the covariables selected and the SPDE approach.

Table 1 shows the mean, median, standard deviation, and the quantiles 0.025 and 0.975, which corresponds to the 95% credible interval of the marginal posterior distribution of the fixed effects. Regarding the influence of canopy cover on LST, that is, cooling capacity, the model shows the biggest negative association among fixed effects. Even though no causal statements can be developed, the model shows that increasing the canopy cover in an observational unit by 450 m^2 is related to a reduction in its LST of about 0.268°C [0.241, 0.295] if ceteris paribus, that is, holding the rest of the

TABLE 1 Numerical summary of the marginal posterior distribution of the fixed effects for the selected model. For each variable, the mean, standard deviation (SD), median ($Q_{0.5}$), and 2.5% ($Q_{0.025}$) and 97.5% quantiles ($Q_{0.975}$) are provided, containing 95% of the probability under the posterior distribution.

Predictor	Mean	SD	$Q_{0.025}$	$Q_{0.5}$	$Q_{0.975}$
Grass cover	−0.098	0.021	−0.139	−0.098	−0.057
Canopy cover	−0.536	0.027	−0.590	−0.536	−0.482
Building area	0.098	0.015	0.068	0.098	0.128
Vacant area	0.141	0.016	0.109	0.141	0.173
Canopy height	0.001	0.004	−0.007	0.001	0.009
Building height	−0.016	0.002	−0.019	−0.016	−0.012
Vacant land	0.111	0.019	0.074	0.111	0.149
Road	0.008	0.016	−0.022	0.008	0.039
Water	0.079	0.074	−0.066	0.079	0.225
Cont. Urb. 80%	−0.073	0.016	−0.105	−0.073	−0.042
Cont. Urb. 50–80%	−0.077	0.017	−0.110	−0.077	−0.043
Cont. Urb. 30–50%	0.084	0.072	−0.058	0.084	0.225
Cont. Urb. 10–30%	−0.152	0.058	−0.267	−0.152	−0.038
Industrial	0.151	0.019	0.114	0.151	0.187

covariables constant. Increasing grass cover, building height, or observational unit being in *a continuous urban fabric with more than 80% sealed surface*, *continuous urban fabric with 50–80% of land sealed*, *or continuous urban fabric with 10–30% of land sealed* are related negatively with LST. Positive associations were found for buildings, vacant area, or observational unit being in a *vacant land or industrial land use*. The model's hyperparameters are listed in Table 2, while checks for biases and prediction errors are presented in Figures S1 and S2.

The INLA-SPDE approach effectively captures and reconstructs the observed spatial pattern of LST (Figure 3). High and low LST regions within the study area are accurately identified by the model (Figure 3b), with uncertainty ranges represented by the quantiles (Figure 3c and d). The model exhibits some over-smoothing of the spatial pattern, leading to less pronounced differences in LST between neighboring areas. This effect is particularly evident because of the increased presence of hotspots within the cooler regions in the northern and northwestern parts of the study area, a common feature of GFs. The lower range of LST values is not accurately modeled. In the actual map (Figure 3a), the minimum temperature is 19.32°C, while the model estimates a minimum of 19.55°C, overestimating LST in the

TABLE 2 Posterior estimates for the model hyperparameters.

Parameter	Mean	Sd.	$Q_{0.025}$	$Q_{0.5}$	$Q_{0.975}$
Precision of the Gaussian likelihood[a]	7.78	0.08	7.62	7.78	7.94
Spatial correlation range (GF)[b]	587.11	45.72	504.34	584.65	684.23
Spatial standard deviation (GF)[c]	1.56	0.09	1.40	1.55	1.74

Note: For each variable, the mean, standard deviation, median ($Q_{0.5}$), 2.5% ($Q_{0.025}$) and 97.5% ($Q_{0.975}$) quantiles are provided, containing 95% of the probability under the posterior distribution of the hyperparameters.

[a]Variability not accounted by the linear predictor of the model and captured in the posterior predictive distribution.

[b]Distance at which the spatial autocorrelation of response variable declines to approximately 0.13 after accounting for the fixed effects.

[c]Variability in response variable attributable to location after accounting for fixed effects.

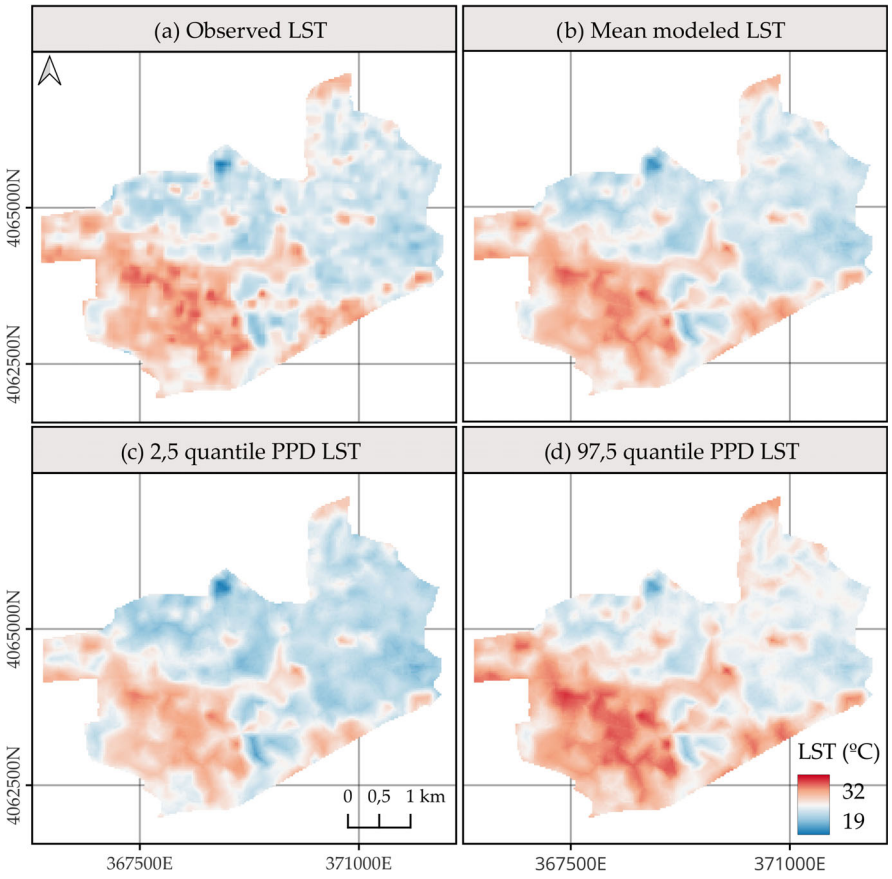

FIGURE 3 (a) Observed spatial pattern of land surface temperature (LST) from Landsat 8 image on August 19, 2022; (b) Mean; (c) Quantile 2.5%; and (d) Quantile 97.5% of the Posterior Predictive Distribution (PPD) of model's prediction of LST. Map represented in coordinate reference system: EPSG 25830.

colder areas of the study region, which corresponds to the water surface situated at the north. However, the model provides accurate predictions for the maximum LST values, located in industrial areas.

4 | DISCUSSION

A BHM to estimate the cooling capacity associated with increasing the tree canopy cover in observational units of 900 m^2 using Landsat 8 LST with the INLA-SPDE approach was carried out. Spatial random effects were included to account for spatial variability in LST remaining after fixed effects inclusion, which may be generated by unmeasured or unmeasurable covariables that vary across the landscape. As the proposed model did not include any variables related to 3D urban geometry apart from mean building height, it is highly likely that the spatial component of the model is related to urban geometry factors and other non-considered covariables.

Urban tree canopy cover has a negative effect on LST, a relationship that has been well-documented by different authors (Guo et al., 2015; Schwaab et al., 2021; Sun et al., 2019). A significant number of studies have relied on proxies for urban tree canopy cover, such as LULC databases or spectral indices. These approaches, along with other statistical learning approaches being used, lead to differences in the estimated cooling capacity. Despite differences, the results are qualitatively similar. As impervious surfaces increase and vegetation cover decreases, sensible heat flux rises and latent heat flux decreases, leading to an increase in LST (Voogt & Oke, 2003). Logan et al. (2020) studied the cooling capacity during day and night using machine learning ensemble methods and showed that as tree canopy increases, the LST decreased up to 10°C. Rosenzweig et al. (2009) estimated a reduction of 0.6°C if canopy cover would be increased to 31% in the city of New York. In a review of articles that studied air temperature reduction by street trees, it was found that an average increase in 10% canopy coverage would reduce air temperature by 0.3°C (Krayenhoff et al., 2021). Air temperatures modeled by LST were found to be reduced by 1°C in European Functional Urban Areas (FUA) by an increase in 16% in tree canopy cover (Marando et al., 2022). Iungman et al. (2023) developed a two step-regression for estimating potential cooling capacity by firstly accounting for LST reduction by urban trees and secondly converting it to air temperature. They estimated that reaching a 30% tree coverage could cool European cities by 0.4°C. Estimates obtained in the present work are relatively lower than those reported in the literature. A cooling potential of 0.16°C [0.144°C, 0.177°C] in LST was estimated for a 30% increase in urban tree canopy cover within an observational unit. These differences may be attributed to multiple factors.

1. Differences in observational units. Previous studies have been developed at the scale of city or FUA; meanwhile in this study, the observational units are 900 m^2 grid cells derived from a pixel-based framework within the city. Literature has demonstrated that different spatial scales can vary the modeled relationship and variable importance (Logan et al., 2020). Weng et al. (2004) observed that the correlations between LST and NDVI as proxy of vegetation cover are higher at smaller pixel sizes. Based on this, it could be expected that analyses conducted at the pixel level, such as the one performed in this study, would report higher estimates compared to city-level analyses, because of the greater variability and differences in LST values at the pixel level. Therefore, the differences in study scale are contrary to the results obtained, suggesting that other factors may play a more significant role in the observed discrepancy.
2. Differences in the response variable. Although Marando et al. (2022), as well as Iungman and colleagues, based their analyses on LST as a primary dataset, their estimates are expressed as predictions of air temperature. As noted by Du et al. (2024), trees have a more pronounced cooling effect on surface temperature than on air temperature. Through the process of transpiration, trees release water vapor, which absorbs heat and cools the surface. This effect is particularly evident at ground level, where evapotranspiration occurs (Berry et al., 2010). While this vapor also influences air temperature, its impact is moderated by atmospheric dynamics (Gunawardena et al., 2017). In addition to transpiration, trees provide shade, reducing the amount of solar radiation that reaches the ground, further contributing to surface cooling. However, air temperature is influenced by broader atmospheric processes, meaning that the shading effect of trees has a more direct impact on LST than on air temperature (Raman et al., 2014). Moreover, trees regulate soil moisture, enhancing surface cooling, with the most significant effects occurring at the surface (Pramova et al., 2012). Given these factors, it is expected that the estimates obtained in this study would be higher than those reported in the literature. This is primarily because of the greater variability of LST and the enhanced capacity of trees to reduce LST compared to air temperature.
3. Differences in scale and coverage. Urban cooling averages at city level imply that urban forests or peri-urban forests are also included in the regression model. Its influence is then captured in the model, increasing the cooling capacity, as expected by large woodland areas. In this case, the study area was entirely urban, with no forested areas present. It implies that only street and park trees are included, which density is notably lower than in natural or seminatural areas, reducing the global cooling potential estimated.
4. Model structure and covariates inclusion. Incorporating factors related to land use, urban geometry in two dimensions, and building height, key determinants of LST distribution, can help refine the estimated cooling effect of urban tree canopy. Becuase no collinearity is observed among the variables, any reduction in the estimated effect when considering only the SPDE component and canopy area would likely stem from omitted variable bias. If omitted covariates are correlated with the variable of interest, the estimated coefficient for the urban canopy contribution becomes a combination of the true effect and the influence of the omitted variables, leading to biased estimates. By including these

covariates in the model, the estimated effect of tree canopy is disentangled from other influencing factors, potentially resulting in a lower but more accurate estimate of its contribution to LST reduction.

5. Spatial confounding is a critical issue in spatial regression models, arising when spatial random effects are not independent of covariates (Dupont et al., 2023). Gilbert et al. (2021) identify four main sources of spatial confounding: (i) omitted confounder bias, which occurs when an unmeasured spatially structured variable influences both the exposure and the outcome; (ii) regularization bias, which stems from finite-sample bias in models using flexible regression functions such as splines or Gaussian processes to control for spatial dependencies; (iii) random effect collinearity, which results from the correlation between spatially dependent random effects and covariates, altering fixed-effect estimates; and (iv) concurvity, which complicates the estimation of an exposure's effect when it closely follows a smooth function of space, particularly when an additional smooth spatial function is included in the model. As noted by Dupont et al. (2023), spatial confounding is particularly problematic when both the covariate and the random effects exhibit smooth spatial patterns, as their collinearity distorts inference on the covariate's effect. In our case, Figure S3 shows that the covariate of interest does not exhibit a smooth spatial pattern, suggesting that the impact of spatial confounding may be limited. Furthermore, recent studies indicate that many methods designed to mitigate spatial confounding can yield counterintuitive results (Khan & Calder, 2022) and have even been classified as "bad statistical practice" (Zimmerman & Ver Hoef, 2022). Despite these concerns, spatial confounding remains an important phenomenon to consider, and future research should explore its integration into models. This is particularly relevant given recent advancements in R-INLA, which are working on the implementation of methods to minimize spatial confounding for geostatistical data, making it a readily accessible tool in practitioners' toolkit (Lamouroux et al., 2024).

Although the estimated effect of tree cover on LST reduction is relatively small compared to the model's RMSE (0.989 ± 0.255°C), as calculated on validation blocks using 10-fold spatial CV, this should not be a concern. Because the 95% credibility interval for the estimated effect of trees does not contain zero and has a range of approximately 0.1°C, we can assert with high probability that there is a negative effect on LST. Furthermore, the reported metrics were calculated on test blocks, which evaluate the model's generalization capability without the influence of the information provided by the spatial autocorrelation of the LST. If these metrics had been computed on the full-data fitted model without CV, we would likely observe an apparent improvement in model performance. However, despite the primary objective of the model being coefficient inference, we consider it essential to report validation metrics on test blocks to prevent overly optimistic assessments of the model's capabilities, as recommended by various authors (e.g., Roberts et al., 2017; Schratz et al., 2019).

Artificial surfaces and urbanization can lead to heat storage (Oke et al., 2017). There is a clear consensus that increasing the building surface area is related to an increase in LST (Peng et al., 2018). Results obtained in this study are in line with previous research. However, there are contradictory results with some LULC categories related to urban uses. In relation to continuous urban fabric uses, we expected higher LST when higher the sealed surface. We found that continuous urban fabric with 80% and 50–80% sealed surface to relate negatively with LST. This can be explained by the influence of 3D urban factors (as discussed in the next paragraph), or by the inclusion of grassy or vacant lands as urban green spaces. The last one may have increased the average LST of the green space category that serves as the model intercept. As previously observed on mediterranean areas during summer, bare soil or vacant lands show the highest LST levels along the different LULC (Unal Cilek & Cilek, 2021). This would explain the increase in LST for LULC category green spaces, making the other LULC categories cooler relatively in comparison to it. Continuous urban fabric with 10–30% sealed surface shows a negative relationship with LST. This can be related to the higher presence of green infrastructure on low density urban lands. As expected, industrial and commercial areas show a positive influence on LST. The relationship between roads and LST shows some uncertainty, despite the expectation of a positive influence. This is likely because of the inclusion of road margins within the road category in the LULC classification. As a result, LST measurements from vegetation along these margins are also included, introducing noise that distorts the true signal associated with the thermal spectrum characteristics of road asphalt.

It is also worth noting that the inconsistency or counterintuitive effects observed for certain LULC categories may be driven by other underlying factors. (1) We believe that the conceptualization of urban fabric categories in the Urban Atlas represents mixtures of land cover types, which can lead to minimal differences in LST between urban fabrics with varying percentages of impervious surfaces. This has also been corroborated in other cities with characteristics very similar to Málaga, such as Valencia (Wei & Sobrino, 2024), where—despite classifying land use into local climate zones (originally developed for LST studies)—a high degree of overlap exists in the statistical distribution of LST across different urban land cover types. (2) The observed relationship might reflect statistical noise, as the remaining covariates may be capturing the effects of these categorical variables, particularly through the inclusion of compositional variables. Although the estimated effects—except for the 30–50% urban fabric category—do not include zero within their credibility intervals, the effect sizes (understood as the mean of the posterior distribution) are small. This suggests that the relationships observed for urban land cover categories may be residual in nature, once spatial effects and other covariates are accounted for.

The impact of the 3D urban landscape, particularly buildings, on LST during the daytime is complex (Kim & Brown, 2021; Lian et al., 2024). While buildings can store heat and release it at night, contributing to higher LST (Chun & Guhathakurta, 2017), they also influence surface roughness during the day. It can modify latent and sensible heat fluxes, which in turn affects urban ventilation generating

mechanical turbulence that enhances convective heat dissipation (He et al., 2019; Huang et al., 2018). Additionally, buildings create shadows that reduce direct sunlight exposure on the ground, leading to lower daytime LST. Numerous studies have shown that lower building density, higher building height, and a higher sky-view factor typically reduce LST (Han et al., 2023). Our model estimated that increasing building surface in an observational unit is related to an increment of LST. Meanwhile, an increase in mean building height in an observational unit is negatively correlated with LST. Effect of building height, even though certainly estimated, has a low effect. This can be related to the fact that we assumed a linear relationship in our model, and according to the literature, building mean height seems to have a nonlinear relationship with LST (Han et al., 2023).

4.1 | Limitations

While the present study has revealed and estimated the local benefits of increasing urban tree canopy coverage, there are several limitations deserving further studies:

1. The model uses LST rather than air temperature. As a result, the cooling potential of the tree canopy is represented by LST, which, although correlated with air temperature, is not a direct measure of thermal comfort perceived by pedestrians. Additionally, there are likely significant differences between the effects of urban trees at canopy level versus ground level that cannot be easily discerned from remotely sensed data because of inherent data limitations. However, the results underscore the importance of vegetated and permeable surfaces at a larger scale, highlighting the need for further investigation into finer urban scales. Understanding these differences will be crucial for informing urban planning strategies aimed at improving thermal comfort in urban spaces.
2. Our model assumes linear relationships between the covariates and LST to derive a simple and interpretable contribution effect of tree canopy cooling capacity for urban planners. However, previous studies have demonstrated that factors influencing LST often exhibit nonlinear relationships. Future research will explore the inclusion of random walk priors for covariate effects within an INLA-SPDE framework to model such nonlinear relationships. Additionally, machine learning has been extensively applied to model the complex relationships involved in SUHI formation. Further studies will investigate the potential of machine learning frameworks to enhance our understanding of these intricate dynamics.
3. Urban heat is influenced by numerous factors, many of which have not been included in the model. Factors, such as sky view, landscape metrics, and relief characteristics, all influence the distribution of LST (Huang et al., 2018; Logan et al., 2020). Additionally, canopy cooling capacity might depend on tree structural and functional traits (e.g., species, leaf size and shape, and crown width) (Miedema-Brown & Anand, 2022; Tamaskani Esfehankalateh et al., 2021). Further research is needed in the field of causal inference to identify and disentangle the most important and causal factors contributing to LST distribution. Such exploration will help develop more robust models, enabling more accurate estimates of the contribution of different variables and their functional relationship with LST. Ultimately, this will provide valuable insights for urban planners, allowing for the implementation of more effective land management strategies and interventions.
4. While the proposed model does not meet causal inference requirements, understanding the urban tree cooling potential, considering urban characteristics that influence LST, can complement and further inform our understanding of the processes that lead to lower urban LST. The results, therefore, have implications for mitigating the SUHIs and preparing urban regions for a warmer climate.

Although a modest reduction in LST is estimated with the proposed model, the cooling effect could improve thermal comfort in cities and prevent a considerable number of deaths. For instance, Royé et al. (2020) estimated city-specific mortality risks for natural causes, finding that increases in temperature from the 1st to the 99th percentile result in the highest mortality risk in Seville (Relative Risk [RR]: 2.73, 95% CI: 2.34–3.18), followed by risks of 1.78 (95% CI: 1.62–1.97) and 1.78 (95% CI: 1.45–2.19) in Barcelona and Bilbao, respectively. Barboza et al. (2021) estimated that 20 deaths per 100,000 inhabitants could be prevented annually if European cities complied with the World Health Organization (WHO) recommendations regarding green space accessibility. The literature strongly emphasizes the urgent need to increase urban greening to improve public health. As Iungman et al. (2023) argue, the full extent of health benefits associated with urban greening should not be assessed solely based on its cooling capacity but rather by considering the broader range of ES it provides. Further studies are necessary to fully assess the comprehensive benefits of incorporating green infrastructure into urban areas. Such analyses should include regulation, provision, supporting and cultural ES to more effectively highlight the potential of urban greening in enhancing environmental quality and creating cities that are healthier, more sustainable, and more resilient to climate change impacts.

AUTHOR CONTRIBUTIONS

Design of the research: Ángel Ruiz-Valero, Álvaro Cortés-Molino, Isidro Martín-Lozano, Jaime Francisco Pereña-Ortiz, and Ángel Enrique Salvo-Tierra. *Performance of the research*: Ángel Ruiz-Valero, Álvaro Cortés-Molino, Isidro Martín-Lozano, Jaime Francisco Pereña-Ortiz, Pablo Cozano-Pérez, Begoña Galindo-Ruiz, Luis Alberto Díaz-Galiano, and Ángel Enrique Salvo-Tierra. *Data analysis*: Ángel Ruiz-Valero, Álvaro Cortés-Molino, Isidro Martín-Lozano, and Jaime Francisco Pereña-Ortiz. *Data interpretation*: Ángel Ruiz-Valero, Álvaro Cortés-Molino, Isidro Martín-Lozano, Jaime Francisco Pereña-Ortiz, Pablo Cozano-Pérez, Begoña Galindo-Ruiz, and Ángel Enrique Salvo-Tierra. *Writing the manuscript*: Ángel Ruiz-Valero and Jaime Francisco Pereña-Ortiz. *Writing – review and editing*: Ángel Ruiz-Valero, Álvaro Cortés-Molino, Isidro Martín-Lozano, Jaime Francisco Pereña-Ortiz, Pablo Cozano-Pérez, Begoña Galindo-Ruiz, Luis Alberto Díaz-Galiano, and Ángel Enrique Salvo-Tierra.

ACKNOWLEDGMENTS

Angel Ruiz Valero was supported by a predoctoral grant financed by the Ministry of Education, Professional Formation and Sport of Spain, in the Program of University Teaching Program (Formacion de Profesorado Universitario, FPU) (FPU22/00067). This work has been a result from "SERVECO: Assessment and Promotion of Ecosystem Services Provided by Urban Trees", a research project funded by the Technological Corporation of Andalusia (CTA) (contract: 8.06/5.03.6083) and developed in collaboration with Althenia S. L. Ángel Ruiz-Valero, Isidro Martín-Lozano, Alvaro Cortés-Molino, Jaime Francisco Pereña-Ortiz, Pablo Cozano-Pérez and Ángel Enrique Salvo Tierra are part of the research team RNM-262: Biogeography, Diversity and Conservation of Junta de Andalucía, Spain. The authors specially want to thank the Málaga City Council for the provision of urban tree inventory in the municipal districts of Bailen-Miraflores, Cruz de Humilladero, and Teati-nos-Universidad.

CONFLICT OF INTEREST STATEMENT

The authors declare that they have no known competing financial interests or personal relationships that could have appeared to influence the work reported in this paper.

DATA AVAILABILITY STATEMENT

These data were derived from the following resources available in the public domain: (Landsat 8, U.S. Geological Survey, https://earthexplorer.usgs.gov/; Aerial orthophotograph and Second Cover aerial-LiDAR, Plan Nacional de Ortofotografía aérea [PNOA, National Plan for Aerial Orthophotography project], https://centrodedescargas.cnig.es/CentroDescargas/home; Cadastral Information, Sede Electrónica del Catastro, https://www.sedecatastro.gob.es/Accesos/SECAccDescargaDatos.aspx; Urban Atlas 2018, Copernicus Land Monitoring Service, 10.2909/fb4dffa1-6ceb-4cc0-8372-1ed354c285e6; OpenStreetMap, 10.32614/CRAN.package.osmdata; and SIOSE-AR, Instituto Geográfico Nacional, https://centrodedescargas.cnig.es/CentroDescargas/home).

ORCID

Ángel Ruiz-Valero https://orcid.org/0009-0006-7790-718X
Jaime Francisco Pereña-Ortiz https://orcid.org/0000-0003-0363-2401
Álvaro Cortés-Molino https://orcid.org/0000-0001-5350-9028
Pablo Cozano-Pérez https://orcid.org/0009-0008-6119-1388
Ángel Enrique Salvo-Tierra https://orcid.org/0000-0002-1464-9770

REFERENCES

Anderson, R. L. (1954). The problem of autocorrelation in regression analysis. *Journal of the American Statistical Association*, *49*(265), 113–129. https://doi.org/10.2307/2281039

Banerjee, S., Carlin, B. P., & Gelfand, A. E. (2014). *Hierarchical modeling and analysis for spatial data* (2nd ed.). Chapman and Hall/CRC. https://doi.org/10.1201/b17115

Barboza, E. P., Cirach, M., Khomenko, S., Iungman, T., Mueller, N., Barrera-Gómez, J., Rojas-Rueda, D., Kondo, M., & Nieuwenhuijsen, M. (2021). Green space and mortality in European cities: A health impact assessment study. *The Lancet Planetary Health*, *5*(10), e718–e730. https://doi.org/10.1016/S2542-5196(21)00229-1

Beck, H. E., McVicar, T. R., Vergopolan, N., Berg, A., Lutsko, N. J., Dufour, A., Zeng, Z., Jiang, X., van Dijk, A. I. J. M., & Miralles, D. G. (2023). High-resolution (1 km) Köppen-Geiger maps for 1901–2099 based on constrained CMIP6 projections. *Scientific Data*, *10*(1), 724. https://doi.org/10.1038/s41597-023-02549-6

Beckett, K. P., Freer-Smith, P. H., & Taylor, G. (1998). Urban woodlands: their role in reducing the effects of particulate pollution. *Environmental Pollution*, *99*(3), 347–360. https://doi.org/10.1016/S0269-7491(98)00016-5

Berry, J. A., Beerling, D. J., & Franks, P. J. (2010). Stomata: key players in the earth system, past and present. *Current Opinion in Plant Biology*, *13*(3), 232–239. https://doi.org/10.1016/j.pbi.2010.04.013

Bolund, P., & Hunhammar, S. (1999). Ecosystem services in urban areas. *Ecological Economics*, *29*(2), 293–301. https://doi.org/10.1016/S0921-8009(99)00013-0

Buyantuyev, A., & Wu, J. (2010). Urban heat islands and landscape heterogeneity: Linking spatiotemporal variations in surface temperatures to land-cover and socioeconomic patterns. *Landscape Ecology*, *25*(1), 17–33. https://doi.org/10.1007/s10980-009-9402-4

Chapman, S., Watson, J. E., Salazar, A., Thatcher, M., & McAlpine, C. A. (2017). The impact of urbanization and climate change on urban temperatures: A systematic review. *Landscape Ecology*, *32*(10), 1921–1935. https://doi.org/10.1007/s10980-017-0561-4

Chun, B., & Guhathakurta, S. (2017). Daytime and nighttime urban heat islands statistical models for Atlanta. *Environment and Planning B: Urban Analytics and City Science*, *44*(2), 308–327. https://doi.org/10.1177/0265813515624685

Diggle, P. J., & Ribeiro, P. J. (2007). *Model-based geostatistics* (1st ed.). Springer Series in Statistics. Springer. https://doi.org/10.1007/978-0-387-48536-2

Du, M., Li, N., Hu, T., Yang, Q., Chakraborty, T. C., Venter, Z., & Yao, R. (2024). Daytime cooling efficiencies of urban trees derived from land surface temperature are much higher than those for air temperature. *Environmental Research Letters*, *19*(4), 044037. https://doi.org/10.1088/1748-9326/ad30a3

Dupont, E., Marques, I., & Kneib, T. (2023). Demystifying spatial confounding. arXiv preprint arXiv:2309.16861. https://doi.org/10.48550/arXiv.2309.16861

European Commission. (2020). EU Biodiversity Strategy for 2030. Communication from the commission to the European parliament, the council, the European economic and social committee and the committee of the regions. Brussels, 20.5.2020. COM(2020) 380 final.

Flintrop, C., Hohlmann, B., Jasper, T., Korte, C., Podlaha, O. G., Scheele, S., & Veizer, J. (1996). Anatomy of pollution; rivers of North Rhine-Westphalia, Germany. *American Journal of Science*, *296*(1), 58–98. https://doi.org/10.2475/ajs.296.1.58

Founda, D., & Santamouris, M. (2017). Synergies between urban heat island and heat waves in Athens (Greece), during an extremely hot summer (2012). *Scientific Reports*, *7*(1), 10973. https://doi.org/10.1038/s41598-017-11407-6

Fox, J., & Weisberg, S. (2019). *An R companion to applied regression* (Third ed.). Sage.

Fuglstad, G. A., Simpson, D., Lindgren, F., & Rue, H. (2019). Constructing priors that penalize the complexity of Gaussian random fields. *Journal of the American Statistical Association*, *114*(525), 445–452. https://doi.org/10.1080/01621459.2017.1415907

Gelman, A., Carlin, J. B., Stern, H. S., & Rubin, D. B. (2013). *Bayesian data analysis* (Third ed.). Chapman and Hall/CRC. https://doi.org/10.1201/b16018

Gilbert, B., Datta, A., Casey, J. A., & Ogburn, E. L. (2021). A causal inference framework for spatial confounding. arXiv preprint arXiv:2112.14946. https://doi.org/10.48550/arXiv.2112.14946

Gunawardena, K. R., Wells, M. J., & Kershaw, T. (2017). Utilising green and bluespace to mitigate urban heat island intensity. *Science of the Total*

Environment, *584-585*, 1040–1055. https://doi.org/10.1016/j.scitotenv.2017.01.158

Guo, G., Wu, Z., Xiao, R., Chen, Y., Liu, X., & Zhang, X. (2015). Impacts of urban biophysical composition on land surface temperature in urban heat island clusters. *Landscape and Urban Planning*, *135*, 1–10. https://doi.org/10.1016/j.landurbplan.2014.11.007

Han, D., An, H., Cai, H., Wang, F., Xu, X., Qiao, Z., Jia, K., Sun, Z., & An, Y. (2023). How do 2D/3D urban landscapes impact diurnal land surface temperature: Insights from block scale and machine learning algorithms. *Sustainable Cities and Society*, *99*, 104933. https://doi.org/10.1016/j.scs.2023.104933

He, B. J., Ding, L., & Prasad, D. (2019). Enhancing urban ventilation performance through the development of precinct ventilation zones: A case study based on the Greater Sydney, Australia. *Sustainable Cities and Society*, *47*, 101472. https://doi.org/10.1016/j.scs.2019.101472

Hou, H., & Estoque, R. C. (2020). Detecting cooling effect of landscape from composition and configuration: An urban heat island study on Hangzhou. *Urban Forestry & Urban Greening*, *53*, 126719. https://doi.org/10.1016/j.ufug.2020.126719

Houghton, R. A., House, J. I., Pongratz, J., van der Werf, G. R., DeFries, R. S., Hansen, M. C., Le Quéré, C., & Ramankutty, N. (2012). Carbon emissions from land use and land-cover change. *Biogeosciences*, *9*(12), 5125–5142. https://doi.org/10.5194/bg-9-5125-2012

Huang, W., Huang, Y., Lin, S., Chen, Z., Gao, B., & Cui, S. (2018). Changing urban cement metabolism under rapid urbanization—A flow and stock perspective. *Journal of Cleaner Production*, *173*, 197–206. https://doi.org/10.1016/j.jclepro.2017.01.008

Imhoff, M. L., Zhang, P., Wolfe, R. E., & Bounoua, L. (2010). Remote sensing of the urban heat island effect across biomes in the continental USA. *Remote Sensing of Environment*, *114*(3), 504–513. https://doi.org/10.1016/j.rse.2009.10.008

IPCC. (2023). In H. Lee & J. Romero (Eds.), *Summary for policymakers. In: Climate change 2023: Synthesis report. Contribution of working groups I, II and III to the sixth assessment report of the Intergovernmental Panel on Climate Change* [Core Writing Team (pp. 1–34). IPCC. https://doi.org/10.59327/IPCC/AR6-9789291691647.001

Iungman, T., Cirach, M., Marando, F., Pereira Barboza, E., Khomenko, S., Masselot, P., Quijal-Zamorano, M., Mueller, N., Gasparrini, A., Urquiza, J., Heris, M., Thondoo, M., & Nieuwenhuijsen, M. (2023). Cooling cities through urban green infra-structure: A health impact assessment of European cities. *The Lancet*, *401*(10376), 577–589. https://doi.org/10.1016/S0140-6736(22)02585-5

Jiménez-Muñoz, J. C., & Sobrino, J. A. (2003). A generalized single-channel method for retrieving land surface temperature from remote sensing data. *Journal of Geophysical Research: Atmospheres*, *108*(D22), 4688. https://doi.org/10.1029/2003JD003480

Khan, K., & Calder, C. A. (2022). Restricted spatial regression methods: Implications for inference. *Journal of the American Statistical Association*, *117*(537), 482–494. https://doi.org/10.1080/01621459.2020.1788949

Kim, S. W., & Brown, R. D. (2021). Urban heat island (UHI) intensity and magnitude estimations: A systematic literature review. *Science of the Total Environment*, *779*, 146389. https://doi.org/10.1016/j.scitotenv.2021.146389

Kong, F., Yin, H., James, P., Hutyra, L. R., & He, H. S. (2014). Effects of spatial pattern of greenspace on urban cooling in a large metropolitan area of eastern China. *Landscape and Urban Planning*, *128*, 35–47. https://doi.org/10.1016/j.landurbplan.2014.04.018

Krayenhoff, E. S., Broadbent, A. M., Zhao, L., Georgescu, M., Middel, A., Voogt, J. A., Martilli, A., Sailor, D. J., & Erell, E. (2021). Cooling hot cities: A systematic and critical review of the numerical modelling literature. *Environmental Research Letters*, *16*(5), 053007. https://doi.org/10.1088/1748-9326/abdcf1

Lamouroux, J., Geffroy, A., Leblond, S., Meyer, C., & Albert, I. (2024). Addressing spatial confounding in geostatistical regression models: An R-INLA approach. arXiv preprint arXiv:2410.01530. https://doi.org/10.48550/arXiv.2410.01530

Lennon, J. J. (2000). Red-shifts and red herrings in geographical ecology. *Ecography*, *23*(1), 101–113. https://doi.org/10.1111/j.1600-0587.2000.tb00265.x

Li, X., Zhou, Y., Yu, S., Jia, G., Li, H., & Li, W. (2019). Urban heat island impacts on building energy consumption: A review of approaches and findings. *Energy*, *174*, 407–419. https://doi.org/10.1016/j.energy.2019.02.183

Lian, D., Yuan, B., Li, X., Shi, Z., Ma, Q., Hu, T., Miao, S., Huang, J., Dong, G., & Liu, Y. (2024). The c trend of global urbanization-induced impacts on day and night land surface temperature from a time-series perspective. *Sustainable Cities and Society*, *109*, 105521. https://doi.org/10.1016/j.scs.2024.105521

Lindgren, F., Rue, H., & Lindström, J. (2011). An explicit link between Gaussian fields and Gaussian Markov random fields: the stochastic partial differential equation approach. *Journal of the Royal Statistical Society, Series B: Statistical Methodology*, *73*(4), 423–498. https://doi.org/10.1111/j.1467-9868.2011.00777.x

Logan, T. M., Zaitchik, B., Guikema, S., & Nisbet, A. (2020). Night and day: The influence and relative importance of urban characteristics on remotely sensed land surface temperature. *Remote Sensing of Environment*, *247*, 111861. https://doi.org/10.1016/j.rse.2020.111861

Marando, F., Heris, M. P., Zulian, G., Udías, A., Mentaschi, L., Chrysoulakis, N., Parastatidis, D., & Maes, J. (2022). Urban heat island mitigation by green infrastructure in European functional urban areas. *Sustainable Cities and Society*, *77*, 103564. https://doi.org/10.1016/j.scs.2021.103564

Miedema-Brown, L., & Anand, M. (2022). Plant functional traits as measures of ecosystem service provision. *Ecosphere*, *13*(2), e3930. https://doi.org/10.1002/ecs2.3930

Molnar, C. (2022). *Interpretable machine learning: A guide for making black box models explainable* (2nd ed.). Institute of Geography (NIG) (2017). Sistema de Ocupación del Suelo de España de Alta Resolucion [Cartografía Digital]. Málaga. https://www.siose.es/siose-alta-resolucion. https://christophm.github.io/interpretable-ml-book/National Accessed: October 2024

National Institute of Geography (NIG). (2022). Plan Nacional de Ortofotografía Aérea (PNOA) /Plan Nacional de Observación del Territorio (PNOT). Retrieved October 2024, from https://pnoa.ign.es/

National Institute of Statistics (NIE). (2022). National Institute of Statistics Population by Cities. Malaga (Spain) (2022). Retrieved October 2024, from https://www.ine.es/dyngs/INEbase/en/categoria.htm?c=Estadistica_P&cid=1254734710990

National Institute of Statistics (NIE). (2023). Cifras oficiales de población de los municipios españoles en aplicación de la Ley de Bases del Régimen Local (Art. 17). Detalle municipal: Málaga. Población por municipios y sexo. Unidades: Personas. Retrieved Accessed: October 2024, from https://www.ine.es/dynt3/inebase/index.htm?padre=525

National Institute of Geography (NIG). (2017). SIOSE AR: Sistema de Información de Ocupación del Suelo de España de Alta Resolucion, versión 2017. Instituto Geográfico Nacional, España. Retrieved September 2024, from https://www.siose.es/

Nieuwenhuijsen, M. J., Dadvand, P., Marquez, S., Bartoll, X., Barboza, E. P., Cirach, M., Borrell, C., & Zijlema, W. L. (2022). The evaluation of the 3-30-300 green space rule and mental health. *Environmental Research*, *215*, 114387. https://doi.org/10.1016/j.envres.2022.114387

Oke, T. R., Mills, G., Christen, A., & Voogt, J. A. (2017). *Urban climates*. Cambridge university press. https://doi.org/10.1017/9781139016476

Padgham, M., Rudis, B., Lovelace, R., & Salmon, M. (2017). osmdata. *Journal of Open Source Software*, *2*(14), 305. https://doi.org/10.21105/joss.00305

Pebesma, E. J. (2004). Multivariable geostatistics in S: The gstat package. *Computers & Geosciences*, *30*(7), 683–691. https://doi.org/10.1016/j.cageo.2004.03.012

Peng, J., Jia, J., Liu, Y., Li, H., & Wu, J. (2018). Seasonal contrast of the dominant factors for spatial distribution of land surface temperature in urban areas. *Remote Sensing of Environment*, *215*, 255–267. https://doi.org/10.1016/j.rse.2018.06.010

Phelan, P. E., Kaloush, K., Miner, M., Golden, J., Phelan, B., Silva, H. III, & Taylor, R. A. (2015). Urban heat island: Mechanisms, implications, and possible remedies. *Annual Review of Environment and Resources*, *40*(1), 285–307. https://doi.org/10.1146/annurev-environ-102014-021155

Picot, X. (2004). Thermal comfort in urban spaces: Impact of vegetation growth: Case study: Piazza della Scienza, Milan, Italy. *Energy and Buildings*, *36*(4), 329–334. https://doi.org/10.1016/j.enbuild.2004.01.044

Pramova, E., Locatelli, B., Djoudi, H., & Somorin, O. A. (2012). Forests and trees for social adaptation to climate variability and change. *Wiley Interdisciplinary Reviews: Climate Change*, *3*(6), 581–596. https://doi.org/10.1002/wcc.195

Raman, A. P., Anoma, M. A., Zhu, L., Rephaeli, E., & Fan, S. (2014). Passive radiative cooling below ambient air temperature under direct sunlight. *Nature*, *515*(7528), 540–544. https://doi.org/10.1038/nature13883

Roberts, D. R., Bahn, V., Ciuti, S., Boyce, M. S., Elith, J., Guillera-Arroita, G., Hauenstein, S., Lahoz-Monfort, J. J., Schröder, B., Thuiller, W., Warton, D. I., Wintle, B. A., Hartig, F., & Dormann, C. F. (2017). Cross-validation strategies for data with temporal, spatial, hierarchical, or phylogenetic structure. *Ecography*, *40*(8), 913–929. https://doi.org/10.1111/ecog.02881

Rosenzweig, C., Solecki, W. D., Parshall, L., Lynn, B., Cox, J., Goldberg, R., Hodges, S., Gaffin, S., Slosberg, R. B., Savio, P., Dunstan, F., & Watson, M. (2009). Mitigating New York City's heat island: Integrating stakeholder perspectives and scientific evaluation. *Bull. Amer. Meteorol. Soc.*, *90*, 1297–1312. https://doi.org/10.1175/2009BAMS2308.1

Rosenzweig, C., Solecki, W. D., Romero-Lankao, P., Mehrotra, S., Dhakal, S., & Ibrahim, S. A. (2018). *Climate change and cities: Second assessment report of the urban climate change research network* (pp. 17–42). Cambridge University Press. https://doi.org/10.1017/9781316563878

Royé, D., Codesido, R., Tobías, A., & Taracido, M. (2020). Heat wave intensity and daily mortality in four of the largest cities of Spain. *Environmental Research*, *182*, 109027. https://doi.org/10.1016/j.envres.2019.109027

Rue, H., Martino, S., & Chopin, N. (2009). Approximate Bayesian inference for latent Gaussian models by using integrated nested Laplace approximations. *Journal of the Royal Statistical Society, Series B: Statistical Methodology*, *71*(2), 319–392. https://doi.org/10.1111/j.1467-9868.2008.00700.x

Schratz, P., Muenchow, J., Iturritxa, E., Richter, J., & Brenning, A. (2019). Hyperparameter tuning and performance assessment of statistical and machine-learning algorithms using spatial data. *Ecological Modelling*, *406*, 109–120. https://doi.org/10.1016/j.ecolmodel.2019.06.002

Schwaab, J., Meier, R., Mussetti, G., Seneviratne, S., Bürgi, C., & Davin, E. L. (2021). The role of urban trees in reducing land surface temperatures in European cities. *Nature Communications*, *12*(1), 6763. https://doi.org/10.1038/s41467-021-26768-w

Sede Electrónica del Catastro (SEC). (2025). Difusión de datos catastrales. Retrieved October 2024, from https://www.sedecatastro.gob.es/Accesos/SECAccDescargaDatos.aspx

Sekertekin, A., & Bonafoni, S. (2020). Land surface temperature retrieval from Landsat 5, 7, and 8 over rural areas: Assessment of different retrieval algorithms and emissivity models and toolbox implementation. *Remote Sensing*, *12*(2), 294. https://doi.org/10.3390/rs12020294

Seto, K. C., Güneralp, B., & Hutyra, L. R. (2012). Global forecasts of urban expansion to 2030 and direct impacts on biodiversity and carbon pools. *Proceedings of the National Academy of Sciences*, *109*(40), 16083–16088. https://doi.org/10.1073/pnas.1211658109

Shaikh, S. F. E. A., See, S. C., Richards, D., Belcher, R. N., Grêt-Regamey, A., Galleguillos Torres, M., & Carrasco, L. R. (2021). Accounting for spatial autocorrelation is needed to avoid misidentifying trade-offs and bundles among ecosystem services. *Ecological Indicators*, *129*, 107992. https://doi.org/10.1016/j.ecolind.2021.107992

Sobrino, J. A., Jimenez-Munoz, J. C., Soria, G., Romaguera, M., Guanter, L., Moreno, J., Plaza, A., & Martinez, P. (2008). Land surface emissivity retrieval from different VNIR and TIR sensors. *IEEE Transactions on Geoscience and Remote Sensing*, *46*, 316–327. https://doi.org/10.1109/TGRS.2007.904834

Stovin, V. R., Jorgensen, A., & Clayden, A. (2008). Street trees and stormwater management. *Arboricultural J.*, *30*(4), 297–310. https://doi.org/10.1080/03071375.2008.9747509

Sun, Y., Gao, C., Li, J., Wang, R., & Liu, J. (2019). Quantifying the effects of urban form on land surface temperature in subtropical high-density urban areas using machine learning. *Remote Sensing*, *11*(8), 959. https://doi.org/10.3390/rs11080959

Tamaskani Esfehankalateh, A., Ngarambe, J., & Yun, G. Y. (2021). Influence of tree canopy coverage and leaf area density on urban heat island mitigation. *Sustainability*, *13*(13), 7496. https://doi.org/10.3390/su13137496

Unal Cilek, M., & Cilek, A. (2021). Analyses of land surface temperature (LST) variability among local climate zones (LCZs) comparing Landsat-8 and ENVI-met model data. *Sustainable Cities and Society*, *69*, 102877. https://doi.org/10.1016/j.scs.2021.102877

United Nations, UN. (2023). Independent Group of Scientists appointed by the Secretary-General, Global Sustainable Development Report 2023: Times of crisis, times of change: Science for accelerating transformations to sustainable development. https://sustainabledevelopment.un.org/content/documents/24797GSDR_report_2019.pdf

United Nations, UN. (2025). United Nations Trade & Development (UNCTAD) Data Hub. Total and urban population, annual. Retrieved 02/03/2025. [dataset] from https://unctadstat.unctad.org/datacentre/dataviewer/US.PopTotal

Valavi, R., Elith, J., Lahoz-Monfort, J. J., & Guillera-Arroita, G. (2019). blockCV: An R package for generating spatially or environmentally separated folds for k-fold cross-validation of species distribution models. *Methods in Ecology and Evolution*, *10*(2), 225–232. https://doi.org/10.1111/2041-210X.13107

Voogt, J. A., & Oke, T. R. (2003). Thermal remote sensing of urban climates. *Remote Sensing of Environment*, *86*(3), 370–384. https://doi.org/10.1016/s0034-4257(03)00079-8

Watanabe, S. (2010). asymptotic equivalence of bayes cross validation and widely applicable information criterion in singular learning theory. *The Journal of Machine Learning Research*, *11*, 3571–3594.

Wei, L., & Sobrino, J. A. (2024). Surface urban heat island analysis based on local climate zones using ECOSTRESS and Landsat data: A case study of Valencia city (Spain). *International Journal of Applied Earth Observation and Geoinformation*, *130*, 103875. https://doi.org/10.1016/j.jag.2024.103875

Wei, T., & Simko, V. (2024). R package 'corrplot': Visualization of a correlation matrix. (Version 0.95). https://github.com/taiyun/corrplot

Weng, Q., Lu, D., & Schubring, J. (2004). Estimation of land surface temperature–vegetation abundance relationship for urban heat island studies. *Remote Sensing of Environment*, *89*(4), 467–483. https://doi.org/10.1016/j.rse.2003.11.005

Wulder, M. A., Roy, D. P., Radeloff, V. C., Loveland, T. R., Anderson, M. C., Johnson, D. M., Healey, S., Zhu, Z., Scambos, T. A., Pahlevan, N., Hansen, M., Gorelick, N., Crawford, C. J., Masek, J. G., Hermosilla, T., White, J. C., Belward, A. S., Schaaf, C., Woodcock, C. E., … Cook, B. D. (2022). Fifty years of Landsat science and impacts. *Remote Sensing of Environment*, *280*, 113195. https://doi.org/10.1016/j.rse.2022.113195

Yu, Z., Yang, G., Zuo, S., Jørgensen, G., Koga, M., & Vejre, H. (2020). Critical review on the cooling effect of urban blue-green space: A threshold-size perspective. *Urban Forestry & Urban Greening*, *49*, 126630. https://doi.org/10.1016/j.ufug.2020.126630

Zimmerman, D. L., & Ver Hoef, J. M. (2022). On deconfounding spatial confounding in linear models. *The American Statistician*, *76*(2), 159–167. https://doi.org/10.1080/00031305.2021.1946149

SUPPORTING INFORMATION

Additional supporting information can be found online in the Supporting Information section at the end of this article.

How to cite this article: Ruiz-Valero, Á., Pereña-Ortiz, J. F., Martín-Lozano, I., Cortés-Molino, Á., Cozano-Pérez, P., Galindo-Ruiz, B., Díaz-Galiano, L. A., & Salvo-Tierra, Á. E. (2025). Quantifying urban tree canopy cooling capacity using Bayesian hierarchical models and satellite imagery. *Plants, People, Planet*, 1–15. https://doi.org/10.1002/ppp3.70085